



Chinese Pharmaceutical Association  
Institute of Materia Medica, Chinese Academy of Medical Sciences

Acta Pharmaceutica Sinica B

[www.elsevier.com/locate/apsb](http://www.elsevier.com/locate/apsb)  
[www.sciencedirect.com](http://www.sciencedirect.com)



ORIGINAL ARTICLE

# EHMT2 promotes tumorigenesis in *GNAQ/11*-mutant uveal melanoma *via* ARHGAP29-mediated RhoA pathway



Yongyun Li<sup>a,b,†</sup>, Tianyu Zhu<sup>a,b,†</sup>, Jie Yang<sup>a,b,†</sup>, Qianqian Zhang<sup>c</sup>,  
Shiqiong Xu<sup>a,b</sup>, Shengfang Ge<sup>a,b</sup>, Renbing Jia<sup>a,b,\*</sup>, Jianming Zhang<sup>d,\*</sup>,  
Xianqun Fan<sup>a,b,\*</sup>

<sup>a</sup>Department of Ophthalmology, Ninth People's Hospital, Shanghai Jiao Tong University School of Medicine, Shanghai 200001, China

<sup>b</sup>Shanghai Key Laboratory of Orbital Diseases and Ocular Oncology, Shanghai 200001, China

<sup>c</sup>National Research Center for Translational Medicine (Shanghai), State Key Laboratory of Medical Genomics, Shanghai Institute of Hematology, Ruijin Hospital, Shanghai Jiao Tong University School of Medicine, Shanghai 200025, China

<sup>d</sup>Institute of Translational Medicine, Zhangjiang Institute for Advanced Study, Shanghai Jiao Tong University, Shanghai 200240, China

Received 6 September 2023; received in revised form 30 October 2023; accepted 2 December 2023

## KEY WORDS

Uveal melanoma;  
EHMT2;  
RhoA pathway;  
ARHGAP29;  
G protein;  
GNAQ;  
GNA11

**Abstract** Constitutive activation of *GNAQ/11* is the initiative oncogenic event in uveal melanoma (UM). Direct targeting *GNAQ/11* has yet to be proven feasible as they are vital for a plethora of cellular functions. In search of genetic vulnerability for UM, we found that inhibition of euchromatic histone lysine methyltransferase 2 (EHMT2) expression or activity significantly reduced the proliferation and migration capacity of cancer cells. Notably, elevated expression of EHMT2 had been validated in UM samples. Furthermore, Kaplan–Meier survival analysis indicated high EHMT2 protein level was related to poor recurrence-free survival and a more advanced T stage. Chromatin immunoprecipitation sequencing analysis and the following mechanistic investigation showed that *ARHGAP29* was a downstream target of EHMT2. Its transcription was suppressed by EHMT2 in a methyltransferase-dependent pattern in *GNAQ/11*-mutant UM cells, leading to elevated RhoA activity. Rescuing constitutively active RhoA in UM cells lacking EHMT2 restored oncogenic phenotypes. Simultaneously blocking EHMT2 and *GNAQ/11* signaling *in vitro* and *in vivo* showed a synergistic effect on UM growth,

\*Corresponding authors.

E-mail addresses: [renbingjia@sjtu.edu.cn](mailto:renbingjia@sjtu.edu.cn) (Renbing Jia), [jzuc@shsmu.edu.cn](mailto:jzuc@shsmu.edu.cn) (Jianming Zhang), [fanxq@sjtu.edu.cn](mailto:fanxq@sjtu.edu.cn) (Xianqun Fan).

†These authors made equal contributions to this work.

Peer review under the responsibility of Chinese Pharmaceutical Association and Institute of Materia Medica, Chinese Academy of Medical Sciences.

<https://doi.org/10.1016/j.apsb.2023.12.002>

2211-3835 © 2024 The Authors. Published by Elsevier B.V. on behalf of Chinese Pharmaceutical Association and Institute of Materia Medica, Chinese Academy of Medical Sciences. This is an open access article under the CC BY-NC-ND license (<http://creativecommons.org/licenses/by-nc-nd/4.0/>).

suggesting the driver role of these two key molecules. In summary, our study shows evidence for an epigenetic program of EHMT2 regulation that influences UM progression and indicates inhibiting EHMT2 and MEK/ERK simultaneously as a therapeutic strategy in *GNAQ/11*-mutant UM.

© 2024 The Authors. Published by Elsevier B.V. on behalf of Chinese Pharmaceutical Association and Institute of Materia Medica, Chinese Academy of Medical Sciences. This is an open access article under the CC BY-NC-ND license (<http://creativecommons.org/licenses/by-nc-nd/4.0/>).

## 1. Introduction

Uveal melanoma (UM) is a rare malignancy that is distinct from its cutaneous counterpart, most occurring between the ages of 50–70 and accounting for 5% of melanoma<sup>1,2</sup>. About half of patients will develop metastatic lesions, predominately in the liver<sup>3</sup>. Once metastases occur, the median progression-free survival is 3.3 months, and the median overall survival is 10.2 months<sup>4</sup>. About 80% of UM is initiated by guanine nucleotide-binding protein G(q) subunit alpha (GNAQ) or guanine nucleotide-binding protein G (11) subunit alpha (GNA11) mutation, whereas cutaneous melanoma is often induced by a *BRAF* or *NRAS* mutation<sup>5</sup>. The continuously activated GNAQ or GNA11 drive multiple signaling including MAPK/MEK/ERK, PI3K/Akt/mTOR, and Rho/Rac/YAP pathways<sup>6</sup>. However, direct targeting GNAQ/11 is extremely challenging. First of all, unlike kinases, there are no obvious druggable pockets available in GTPases. Second, the crucial role of GNAQ/11 involved in normal physiological function might limit the therapeutical window. Early studies show GNAQ class of G proteins is essential in cardiac growth and development in mice<sup>7</sup>. Till now, the only GNAQ/11 inhibitors identified are two natural products (YM-254890, FR900359) and two imidazopiperazine derivatives (GQ262, GQ127), specifically inhibiting GNAQ/11-mediated signal transduction in *GNAQ/11*<sup>Q209</sup>-mutant UM cells<sup>8–11</sup>. Alternatively, targeting GNAQ/11 downstream signaling pathways often fails due to the rapid emergence of drug resistance. For instance, the most studied MEK inhibitors in clinical trials often get poor response among UM patients<sup>12</sup>. This raises the question of whether direct downstream targets can be suppressed to provide long-term benefits, or whether the *GNAQ/11*-mutant UM has some unknown genetic vulnerabilities that can be effectively used as drug targets.

We and others recently reveal that Trio/Rho/Rac/YAP signaling has played a critical role in tumorigenesis and could be used as therapeutic targets in UM<sup>13,14</sup>. The constitutive activation of GNAQ/11 is the oncogenic driving force triggering YAP-dependent gene transcription, *via* increasing YAP translocation into the cellular nucleus. This process requires the activation of Trio, as well as the following involvement of the small GTPases RhoA, and Rac1, instead of through the classic PLC $\beta$  stimulation<sup>13</sup>. YAP is localized in the cellular nucleus and is activated in *GNAQ/11*-mutant UM. Inhibiting YAP *via* pharmacological or genetic approaches could block the progression of UM tumors harboring *GNAQ/11* mutation *in vivo*<sup>15</sup>. Additionally, we found that *GNAQ/11*-mutant UM is extremely sensitive to metabolic stress. The copper ionophore elesclomol could effectively inhibit YAP signaling pathways by raising intracellular ROS level through directly targeting mitochondria<sup>14</sup>.

Those observations pose a question of whether *GNAQ/11*-mutant UM has a distinct metabolic reprogramming under the influence of epigenetic changes. Indeed, multiple lines of evidence

underscore the importance of epigenetic alteration during UM process. For example, a significant difference in the global level of histone acetylation between UM tumors and healthy controls, especially histone 3 acetylation<sup>16</sup>. In two cohorts, the presence of a T-cell infiltrate is positively correlated with the expression of HDACs<sup>17</sup>. In UM, histone methyltransferase EZH2 is involved in the downregulation of IFN- $\gamma$ -induced transcription of CIITA<sup>18</sup>. Besides, it increases the percentage and self-renewal capacity of cancer stem-like cells and facilitates the invasion activity of UM cells through RhoGDI $\gamma$ -Rac1 axis<sup>19</sup>. Nevertheless, a novel epigenetic program that is vital to UM progression remains to be identified. Here, we first proposed the hypothesis that euchromatic histone lysine methyltransferase 2 (EHMT2, also named G9a) was upregulated in UM, based on the results of high-throughput screening (HTS) on UM cell proliferation by using in-house functional chemical probes and gene expression profiling data from UM clinical datasets. We revealed that EHMT2 inhibitors suppressed *GNAQ/11*-mutant UM cell growth and invasiveness through regulating the expression of GTPase-activating protein ARHGAP29 and the activity of RhoA signaling pathway. Our findings suggest an effective strategy for UM intervention by inhibiting EHMT2 and MEK/ERK signaling simultaneously.

## 2. Materials and methods

### 2.1. Ethical disclosure

Written informed consents were obtained from patients, whose tissue was used for patient patient-derived xenograft (PDX) model. The experimental procedures were reviewed and approved by the ethics committee of Shanghai Ninth People's Hospital (reference number: 20216342) and Shanghai Ninth People's Hospital Central Lab IACUC (Permit Number: SYXK (Shanghai) 2016–0016). The procedures of animal experiments complied with the Declaration of Helsinki.

### 2.2. Cell lines

Cell lines 92.1, OMM2.3, OMM1, Mel285, and Mel290 were kindly provided by Prof. Martine J. Jager (Leiden University Medical Center)<sup>20–25</sup>. 92.1, OMM2.3, OMM1, Mel285, Mel290, and MUM2B were cultured in Roswell Park Memorial Institute (RPMI, Gibco) 1640 containing 10% fetal bovine serum (FBS) in the presence of penicillin/streptomycin. The human cutaneous melanocyte cell line PIG1 was a kind gift from Prof. Caroline Le Poole (Loyola University)<sup>26</sup>, cultured in Median 254 (Gibco) containing 1% Human Melanocyte Growth Supplement (HMGS, Gibco) and 10% FBS. Cells were cultured in a humidified incubator at 37 °C with 5% CO<sub>2</sub>.

### 2.3. Orthotopic and subcutaneous mouse models

Five-week-old male BALB/c nude mice were obtained from Shanghai Jie Si Jie Laboratory Animals Co. Ltd. and used in this study. Chloral hydrate was used to anesthetize them.

For orthotopic models, after the cornea was anesthetized with Benoxil, a surgical microscope was used to perform injections.  $2 \times 10^4$  sgScr or sgEHMT2 OMM2.3 cells or luciferase-labeled 92.1 cells were diluted with 2  $\mu$ L PBS and microinjected into the subchoroidal space of an eyeball with a Hamilton syringe. The control group was not injected with any UM cells. Antibiotic eye ointment was applied to avoid ocular inflammation. After 21 days, control animals and animals infected with sgScr or sgEHMT2 OMM2.3 cells were euthanized, and UM samples were obtained before being fixed in paraformaldehyde.

For PDX, tumor tissue from a *GNAQ*<sup>Q209L</sup>-mutant patient was obtained and subcutaneously implanted into the right flank of mice. The volume of tumors was calculated as follow: width<sup>2</sup>  $\times$  length  $\times$  0.52.

### 2.4. Xenograft models in zebrafish

The UM xenograft model in zebrafish was established following the protocol reported previously using 92.1 cells<sup>14</sup>. Drug administration started at 24 hpi (hour post injection). Concentrations of BIX01294, binimetinib, and ulixertinib were determined according to the result of safety test ( $n = 15$ ). Stereo images and confocal photos were acquired with a stereomicroscope (Nikon SMZ25) and confocal microscope (Phenix) and processed with ImageJ.

### 2.5. EHMT2 inhibitor combined with MEK/ERK inhibitor efficacy studies

BIX01294, UNC0631, binimetinib, and ulixertinib were purchased from Selleck Chemicals. In the orthotopic and PDX model, the mice were divided into six groups: the vehicle group ( $n = 6$ ), the UNC0631 group ( $n = 6$ , 5 mg/kg, qd, i.p.), the binimetinib group ( $n = 6$ , 3 mg/kg, qd, i.g.), the ulixertinib group ( $n = 6$ , 50 mg/kg, i.g., qd), the UNC0631 + binimetinib group and the UNC0631 + ulixertinib group. Treatment lasted for 21 days. For the orthotopic model, bioluminescence was measured using an *in vivo* small animal imaging system. The tumor samples were collected after the mice were euthanized.

### 2.6. High-throughput screening (HTS)

Three annotated libraries containing 3541 compounds were tested in six UM cell lines using an automated platform, following the protocol reported previously<sup>14</sup>.

For combined drug screening, one annotated library with a total of 2103 compounds was used. OMM2.3 were seeded into 384-well plates either applied with 2  $\mu$ mol/L of individual compound or combined with 2  $\mu$ mol/L BIX01294. After 72 h, cell viability was determined *via* CellTiter-Glo Luminescent assay. The ratio of the number of drugs with 50% killing efficacy to the total number of drugs at the same target was calculated and recorded in [Supporting Information Table S1](#).

### 2.7. Patient samples and immunofluorescence (IF)

A cohort containing human specimens of 83 ocular melanoma and 27 nevus was collected from 2007 to 2017 in Ninth People's Hospital, Shanghai Jiao Tong University School of Medicine. The information of patients has been described previously<sup>27</sup>. Specimens were collected following the approved procedure from consenting patients. After the slides were deparaffinized and rehydrated, Na-citrate buffer was used to retrieve the antigen. The slides were incubated with primary antibodies overnight at 4  $^{\circ}$ C, including EHMT2 (Invitrogen, PA5-78347), RhoA-GTP (NewEast Biotechnology, 26904), Ki67 (Cell Signaling, 9449), ARHGAP29 (Santa Cruz, sc-365554). For cell IF, slides were fixed with 4% PFA, permeabilized with 0.3% Triton X-100, and blocked in 5% BSA. They were then incubated in primary antibodies against EHMT2 (Invitrogen, PA5-78347), MITF (Proteintech, 13092-1-AP), TYR (Proteintech, 21995-1-AP), DCT (Abcam, ab74073), YAP (Proteintech, 66900-1-Ig). DAPI (Abcam, ab104139) was used to stain cell nuclei. TUNEL assay was performed according to instructions (Millipore). Image acquisition was conducted *via* an Eclipse 80i Microscope (Nikon, Japan). The clinicopathologic characteristics of UM patients and associations between EHMT2, RhoA-GTP expression are recorded in [Supporting Information Table S2](#).

### 2.8. Western blot (WB)

This assay was conducted following the protocol reported previously<sup>14</sup>. Primary antibodies used: EHMT2 (Invitrogen, PA5-78347), H3K9me2 (Abcam, ab1220), H3 (Proteintech, 17168-1-AP), cyclin D1 (Abcam, ab134175), c-Myc (Abcam, ab32072), Bax (Abcam, ab32503), H3K9me1 (Abcam, ab176880), RhoA (Santa Cruz, sc-418), p-YAP (phospho Ser127, Abcam, ab76252), YAP (Proteintech, 66900-1-Ig), CTGF (Proteintech, 23936-1-AP), GFP (Proteintech, 50430-2-AP), ARHGAP29 (Santa Cruz, sc-365554), MITF (Proteintech, 13092-1-AP), TYR (Proteintech, 21995-1-AP), DCT (Abcam, ab74073), GAPDH (Abcam, ab8245).

### 2.9. Growth kinetic assay *in vitro*, colony formation, cell cycle arrest, and apoptosis detection

For growth kinetic assay, 2000 cells were seeded into each well of 96-well plates. Cell growth was detected every 24 h after seeding with Cell Counting Kit 8 (Dojindo). The absorbance value was detected using a BioTek Epoch 2 microplate reader (BioTek, USA).

For colony formation, cell cycle arrest, and apoptosis detection, the procedures were conducted following the protocol reported previously<sup>14</sup>.

### 2.10. Wound healing assay

$10^6$  cells were seeded in each well of a 6-well plate. The wound was made by sterilized pipette tips after cells attached to the bottom. The medium was replaced with new medium containing 1% FBS. The images of the wounds were captured every 24 h.

### 2.11. Transwell migration assay

The cell migration activity was determined *via* Transwell assay.  $10^4$  cells were seeded into each chamber with 8- $\mu$ m pores containing medium with 1% FBS. The lower well was supplied with 20% FBS. After incubating for 48 h, the cells that migrated out of pores were stained with crystal violet dye. The crystal violet dye was washed with 33% acetic acid and the absorbance of the washed liquid was measured with an Epoch 2 microplate reader (BioTek, USA).

### 2.12. Chromatin immunoprecipitation sequencing (ChIP-seq) and ChIP-qPCR

$10^8$  cells were collected and fixed with 1% formaldehyde. Sonication was conducted on ice for 8 min. The sonicated chromatin was diluted 10-fold before being added with 60  $\mu$ L Protein G Agarose (Millipore, USA). The mixture was shaken at 4 °C for 2 h and briefly centrifuged. The supernatant was transferred into a new tube and incubated with antibodies against EHMT2 (Invitrogen, PA5-78347), H3K9me2 (Abcam, ab1220), and RNA polymerase II (Abcam, ab5095) at 4 °C overnight. Protein was pulled down at 4 °C for 6 h using Protein A and Protein G Magnetic Beads (Millipore, USA). The DNA was released from the chromatin after crosslinking reversal, proteinase K treatment and precipitation. 30 ng DNA was used for library construction for ChIP-seq (New England Biolabs). Libraries were pooled in equimolar, and the sequencing was performed on the Illumina MiSeq (Illumina). The primers used in PCR are listed in Supporting Information Table S3.

### 2.13. RhoA activity detection

RhoA activity in OMM2.3, 92.1 and Mel290 cells, untreated and treated with 2  $\mu$ mol/L BIX01294 and 2  $\mu$ mol/L UNC0631 for 24 h, as well as sgScr and sgEHMT2 cells, OMM2.3 with and without ARHGAP29 overexpression, was determined *via* the Active RhoA Detection Kit (Cell Signaling Technology). GTP $\gamma$ S is used as a positive control to active RhoA. GST-PAK1-PBD fusion protein was applied to bind with the activated GTP-bound RhoA. The complex was then immunoprecipitated *via* glutathione resin by GST-linked protein. After centrifugation and washing off unbound proteins, GTPase was eluted with SDS buffer. The GTP-RhoA was detected through WB using an anti-RhoA antibody (Santa Cruz, sc-418).

### 2.14. Lentivirus packaging and generation of stable cell lines

EHMT2 sgRNAs and scrambled control sequences (sgScr) were cloned into the PGMLV-GM1 vector. The ARHGAP29-Flag open reading frame (ORF) sequence was cloned into the PGMLV-CMV backbone. Lipofectamine 2000 reagent (Invitrogen) was applied to transfect 239T cells with 3  $\mu$ g pMD2.D plasmid, 6  $\mu$ g PsPax plasmid and 3  $\mu$ g indicated plasmid. The above agents were incubated in Opti-MEM I Reduced Serum Medium (GIBCO). After the cells were transfected for 6 h, the medium was replaced. The supernatant was collected and filtered at 48, 72 h, and concentrated with the Lenti-X Concentrator (Takara).

$3 \times 10^5$  cells were seeded into a 60 mm dish (Corning) 24 h before infection, and the medium was substituted with 25  $\mu$ L/mL lentivirus and 10 ng/mL polybrene (Sigma–Aldrich). Stable cell lines were selected 48 h later by puromycin (InvivoGen) and

blasticidin (InvivoGen) for 2 weeks. The concentration of selection was listed in Supporting Information Table S4. For rescue experiments, sgScr, sgEHMT2 and control 92.1 cells were transfected with 2 mg *RhoA-GFP* plasmid (Addgene 12968, pcDNA3-EGFP-RhoA-Q63L). The sequences of the constructed plasmid are listed in Supporting Information Table S5.

### 2.15. RNA extraction and realtime PCR analysis

Total RNA was extracted with Trizol reagent (Takara). cDNA was synthesized using the PrimeScript RT reagent kit (Takara). Real-time PCR was performed by PowerUp SYBR Green Master Mix (Thermo Fisher Scientific) with primers for *GAPDH* and *ARHGAP29* (Table S3).

### 2.16. Data availability

All sequencing data was uploaded to Gene Expression Omnibus (GEO) database by accession PRJNA842784.

### 2.17. Statistical analysis

Statistical analysis was done with GraphPad software. Data was presented as mean  $\pm$  standard error of the mean (SEM). Kaplan–Meier curve was shown by survival plots. Unpaired two-tailed Student's *t*-test and two-way ANOVA were utilized. Correlations were calculated by Pearson's correlation coefficient (*r*) and *P* value. Results were determined statistically significant with \**P* < 0.05, \*\**P* < 0.01, \*\*\**P* < 0.001, and \*\*\*\**P* < 0.0001.

## 3. Results

### 3.1. Identification of EHMT2 as a druggable target of UM

In search of druggable targets of *GNAQ/11*-mutant UM, we performed a cell-based cytotoxicity screen by using an in-house compounds library as a chemical toolbox. Briefly, 3541 compounds with known targets were tested in six UM cell lines at 2  $\mu$ mol/L concentration in a 3-day assay. Among the six cell lines used, 92.1 and OMM2.3 are *GNAQ*<sup>Q209</sup>-mutant, OMM1 carries a *GNAI1*<sup>Q209</sup> mutation, while Mel285, Mel290, MUM2B are *GNAQ/11*-wild type. One category of compounds, known as methyltransferase inhibitors, showed up at the top of the hit list. Particularly, there were four drugs showing strong effect on viability in all the cell lines: JIB-04 (Jumonji demethylase inhibitor), SGI-1027 (DNA methyltransferase inhibitor), BIX01294, and UNC0631 (EHMT2 inhibitors) (Fig. 1A). Further dose–response analysis showed that EHMT2 inhibitors, BIX01294 and UNC0631 efficiently stop UM cells proliferation, with  $-1.294$  and  $-1.368$  of  $\log_2$ FC (fold change, compound/DMSO), respectively (Fig. 1B).

Next, we expanded our investigation by collecting a set of 74 epigenetic modulators to further profile their pharmacological potency against *GNAQ/11*-mutant and -wild type cells by examining the half maximal inhibitory concentration (IC<sub>50</sub>). Again, EHMT2 inhibitors BIX01294 and UNC0631 showed potent efficacy against *GNAQ/11*-mutant UM cells at IC<sub>50</sub> 1.221–3.584 and 0.854–2.184  $\mu$ mol/L, respectively (Fig. 1C). EHMT2 and EHMT1, also known as G9a and GLP, are mainly responsible for the monomethylation and dimethylation of histone H3 lysine 9 (H3K9me1/2) in a wide range of chromosomal regions through

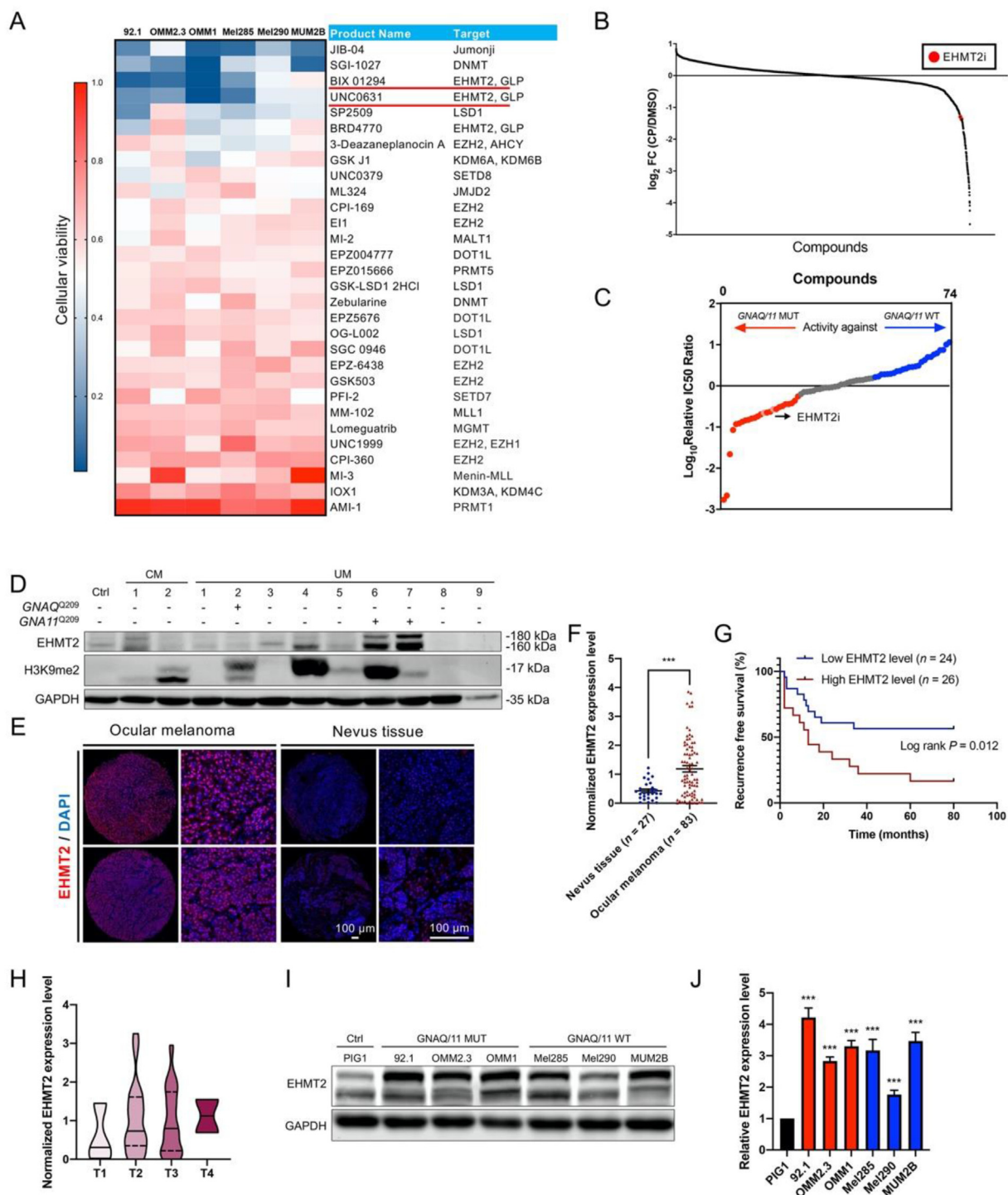


**Figure 1** HTS indicates EHMT2 as a potential target for treating UM. (A) The representative drugs of methyltransferase targets in the HTS library are listed and the cellular viability is illustrated with color. (B) Summary of cell viability upon administration of compounds. The position of EHMT2i is indicated by the red dot. (C) Relative IC<sub>50</sub> ratio of 74 compounds against UM cells on the logarithmic (base 10) scale. The efficacy of compounds against *GNAQ/11*-mutant cells from strong to weak is demonstrated as red, grey and blue dots. (D) The expression level of EHMT2 and H3K9me2 are detected in nine cases of UM, as well as one control choroid tissue and two cases of conjunctival melanoma. (E) EHMT2 staining in the tissue microarray of ocular melanoma and nevus. (F) The fluorescence intensity was quantified by ImageJ. The EHMT2 expression level in a tissue microarray of nevus ( $n = 27$ ) and ocular melanoma ( $n = 83$ ). (G) Kaplan–Meier RFS curve of ocular melanoma patients with EHMT2 high-expression ( $n = 26$ ) and low-expression ( $n = 24$ ), who had complete prognosis data. (H) Violin diagram showing the expression level of EHMT2 categorized according to patients' clinical T stages. (I, J) The expression level of EHMT2 is detected in one control cell PIG1 and six UM cells and quantified with ImageJ. GAPDH is used as the loading control.  $n = 2$  independent experiments for (A),  $n = 3$  independent experiments for (D, I), \* $P < 0.05$ , \*\* $P < 0.01$ , \*\*\* $P < 0.001$ .

their lysine methyltransferase function, leading to transcriptional inhibition of target genes<sup>28</sup>. The dysregulated function of EHMT2 or EHMT1 has been reported in different cancers<sup>29</sup>. For example, EHMT2 epigenetically silenced *RARRES3* expression in hepatocellular carcinoma<sup>30</sup>, *PTEN* in alveolar rhabdomyosarcoma<sup>31</sup>, and the Hippo pathway kinase LATS2, leading to oncogenic activation of YAP in cholangiocarcinoma<sup>32</sup>. This data prompted us to speculate if EHMT2 would be a druggable target in UM.

We immediately examined the expression profiles of EHMT2 in nine UM, two conjunctival melanoma (CM) tumor specimens and six cell lines available in the lab. Western blot analysis showed a higher expression level of EHMT2, as well as its main target for methylation, dimethylated H3K9 (H3K9me2), in three cases of UM and one case of CM (Fig. 1D). Notably, the level of EHMT2 was significantly higher in UM specimens harboring *GNAQ11* mutation than in other samples. Encouraged by the aforementioned data, we performed a large set of IF staining for EHMT2 with tissue microarray and confirmed that EHMT2 was overexpressed in 83 ocular melanoma samples compared to 27 sets of nevus ( $P < 0.001$ ) (Fig. 1E and F). Furthermore, Kaplan–Meier survival analysis of 50 of 83 patients with prognosis data demonstrated that high EHMT2 expression is associated with poorer recurrence-free survival (RFS) ( $P = 0.012$ ) and more advanced T stage (Fig. 1G and H). In addition, the protein level of EHMT2 in UM cells was higher than that in melanocyte cell line PIG1 (Fig. 1I and J). Taken together, we decided to thoroughly investigate the potential oncogenic role of EHMT2 in UM, especially *GNAQ11*-mutant tumors.

### 3.2. EHMT2 regulates UM cell proliferation and migration

To determine the cellular pharmacological properties of EHMT2 inhibition, we first examined  $IC_{50}$  of nine commercially available EHMT2 inhibitors in six UM cell lines and one melanocyte cell line (Supporting Information Fig. S1). BIX01294 and UNC0631 were chosen as pharmacological tools due to their potency and safety margin. Both *GNAQ11*-mutant and -wild type UM cells were arrested in G2/M phase and the proportion of apoptosis was elevated when treated with UNC0631 (Supporting Information Fig. S2A and S2B, Fig. 2A and B). WB analysis showed that EHMT2 inhibition resulted in significant downregulation of c-Myc, cyclin D1, and upregulation of Bax, which were required for cell cycle progression and apoptosis, respectively. Meanwhile, H3K9me2 was downregulated after EHMT2 inhibitors treatment (Fig. 2C).

To further validate these observations, two specific small guide RNAs (sgRNAs) were applied to knockdown EHMT2 in 92.1, OMM2.3 and MUM2B. Compared with parental cells, those cells with suppression of EHMT2 expression led to cell cycle arrest out of the S phase (Fig. S2C, Fig. 2D and E). Silencing EHMT2 decreased the expression level of c-Myc, cyclin D1, H3K9me1, H3K9me2, and increased the expression of Bax (Fig. 2F). Next, we investigated EHMT2's function on migratory and invasive capacity of UM cells by Transwell assay. In the 48-h cell migration assay, compared to control cells, defective cellular mobility was observed upon treatment with BIX01294, as well as in sgEHMT2 cells (Fig. 2G and H).

To our surprise, knocking down EHMT2 enhanced the melanin synthesis of UM cells (Supporting Information Fig. S3A). The expression of microphthalmia transcription factor (MITF), tyrosinase (TYR), and dopachrome tautomerase (DCT), which were required for melanin synthesis, were all upregulated after EHMT2

depletion and inhibition (Fig. S3B–D). To our knowledge, there were no clinical records to show the level of UM pigmentation and the degree of malignancy, such as the tendency of tumor metastasis. However, it is reported that MITF deficiency accelerates *GNAQ*-driven UM<sup>33</sup>.

We further employed a xenograft mouse model to confirm the function of EHMT2 for UM growth *in vivo*. Palpable tumors emerged within 3 weeks after OMM2.3 with different levels of EHMT2 were injected into their eyeballs. Silencing EHMT2 impaired tumor growth (Fig. 2I and J). Therefore, we confirmed that EHMT2 was essential for the promotion of UM growth.

### 3.3. Rho/YAP signaling pathway is regulated by EHMT2 in *GNAQ11*-mutant UM cells

We performed CHIP-seq to gain a full knowledge of genome-wide target genes of EHMT2. EHMT2 occupancy was found to be enriched on promoters, gene bodies, and intergenic regions (Fig. 3A). The peaks were mapped to the transcription start site (TSS) (Fig. 3B). Fig. 3C showed the Top 10 signaling pathways enriched by genes with EHMT2 peaks, indicated by KEGG analysis. Among them, Hippo signaling pathway was closely associated with the metastatic properties of UM, which had been reported to play a significant role in patient mortality<sup>15</sup>. In *GNAQ11* signaling transduction, YAP nuclear translocation required Trio and the subsequent activation of Rho<sup>13</sup>. Besides, Rap1 could block RhoA signal transduction *via* forming a complex with RAS interacting protein 1 (Rasip1), thus inhibiting cell proliferation<sup>34</sup>. Interestingly, Rap1 signaling was also enriched in EHMT2 CHIP-seq. These observations indicated that EHMT2/Rap1/Rho signaling might facilitate YAP-related UM growth. In addition, a CDK7/9 inhibitor, SNS-032, repressed the RhoA GTPase activity, subsequently inhibiting UM cell motility and liver metastasis<sup>35</sup>, which further suggested that RhoA might be a suitable therapeutic target for UM. Therefore, we focused on RhoA/YAP signaling to explore in detail the molecular mechanism of EHMT2 inhibition in UM cells.

In *GNAQ*-wild type UM cells, the RhoA level was almost inactivated, while in *GNAQ*-mutant UM cells, the active RhoA level was largely downregulated upon UNC0631 treatment or EHMT2 knockdown (Fig. 3D and E). Besides, treatment with 2  $\mu\text{mol/L}$  BIX01294 or UNC0631 for 24 h and knockdown of EHMT2 both blocked the nuclear translocation of YAP in *GNAQ*-mutant UM cells, as shown by its decreased cytosolic fraction and increased nuclear fraction, judged by YAP IF detection. However, YAP nuclear translocation was not blocked in *GNAQ*-wild type UM cells (Fig. 3–I). Consequently, the ratio of phosphorylated YAP/total YAP was increased, while the downstream target CTGF was reduced, after BIX01294 or UNC0631 treatment and EHMT2 knockdown in OMM2.3 and OMM1, but not in Mel285 and Mel290 (Fig. 3J and K). These results indicated that EHMT2 regulated cellular activity through Rho/YAP signaling pathway only in *GNAQ11*-mutant UM cells.

### 3.4. Active RhoA restores cell proliferation and motility in EHMT2 knockdown UM cells

We next aimed to check whether the activity of RhoA signaling would be meaningful in promoting UM. The upregulated RhoA signaling has been further confirmed in 83 ocular melanoma specimens by IF staining for RhoA-GTP ( $P < 0.001$ ) (Fig. 4 and B). Kaplan–Meier survival analysis indicated that high RhoA

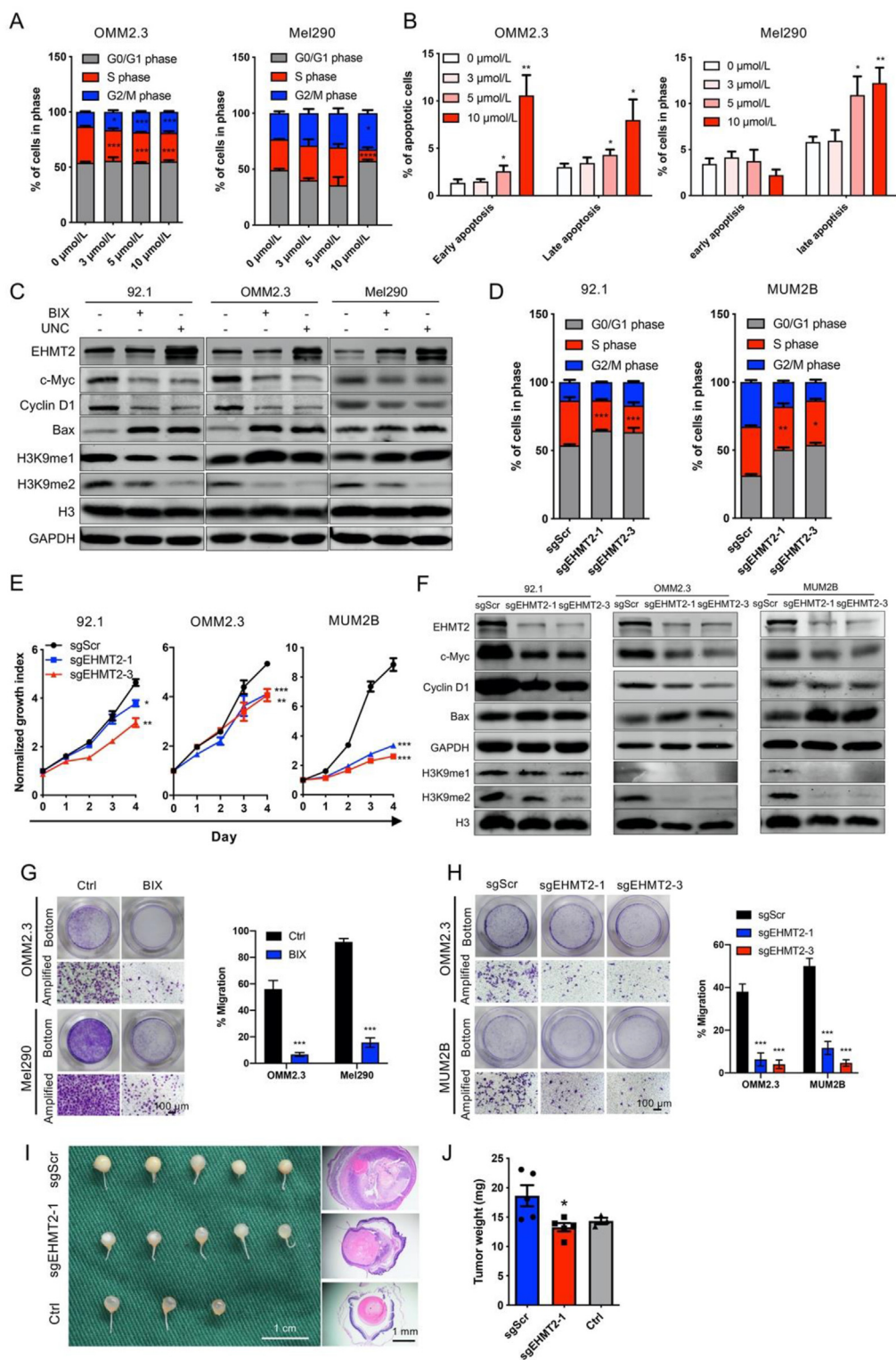


**Figure 2** Inhibiting EHMT2 alters the proliferation and motility of UM. Cell cycle arrest (A) and apoptosis ratio (B) of OMM2.3 and Mel290 treated by UNC0631 for 24 h. (C) WB analysis of c-Myc, cyclin D1, Bax, H3K9me1 and H3K9me2 in UM cells treated for 24 h with BIX01294 (2  $\mu\text{mol/L}$ ) and UNC0631 (2  $\mu\text{mol/L}$ ). (D) Cell cycle distribution of 92.1 and MUM2B with and without stable EHMT2 knockdown. (E) Cell proliferation assay is performed with sgScr and sgEHMT2 UM cells for 4 days. (F) WB analysis of EHMT2, c-Myc, cyclin D1, Bax, H3K9me1 and H3K9me2 in sgScr and sgEHMT2 UM cells. (G) The motility of UM cells treated with DMSO and BIX01294 (2  $\mu\text{mol/L}$ , 48 h) is analyzed by Transwell assay. (H) Motility of sgScr and sgEHMT2 cells. Quantification of data is shown in bar graphs. (I) sgScr and sgEHMT2 UM cells are microinjected into the eyeballs of nude mice. Ctrl group is not injected with any cells. Tumors are harvested 21 days after injection and H&E staining is done. (J) The weight of the eyeballs (with the tumors) was measured 21 days after injection. H3 and GAPDH are used as the loading control for nuclear and cytoplasmic protein respectively.  $n = 3$  independent experiments for (A–H), \* $P < 0.05$ , \*\* $P < 0.01$ , \*\*\* $P < 0.001$ .

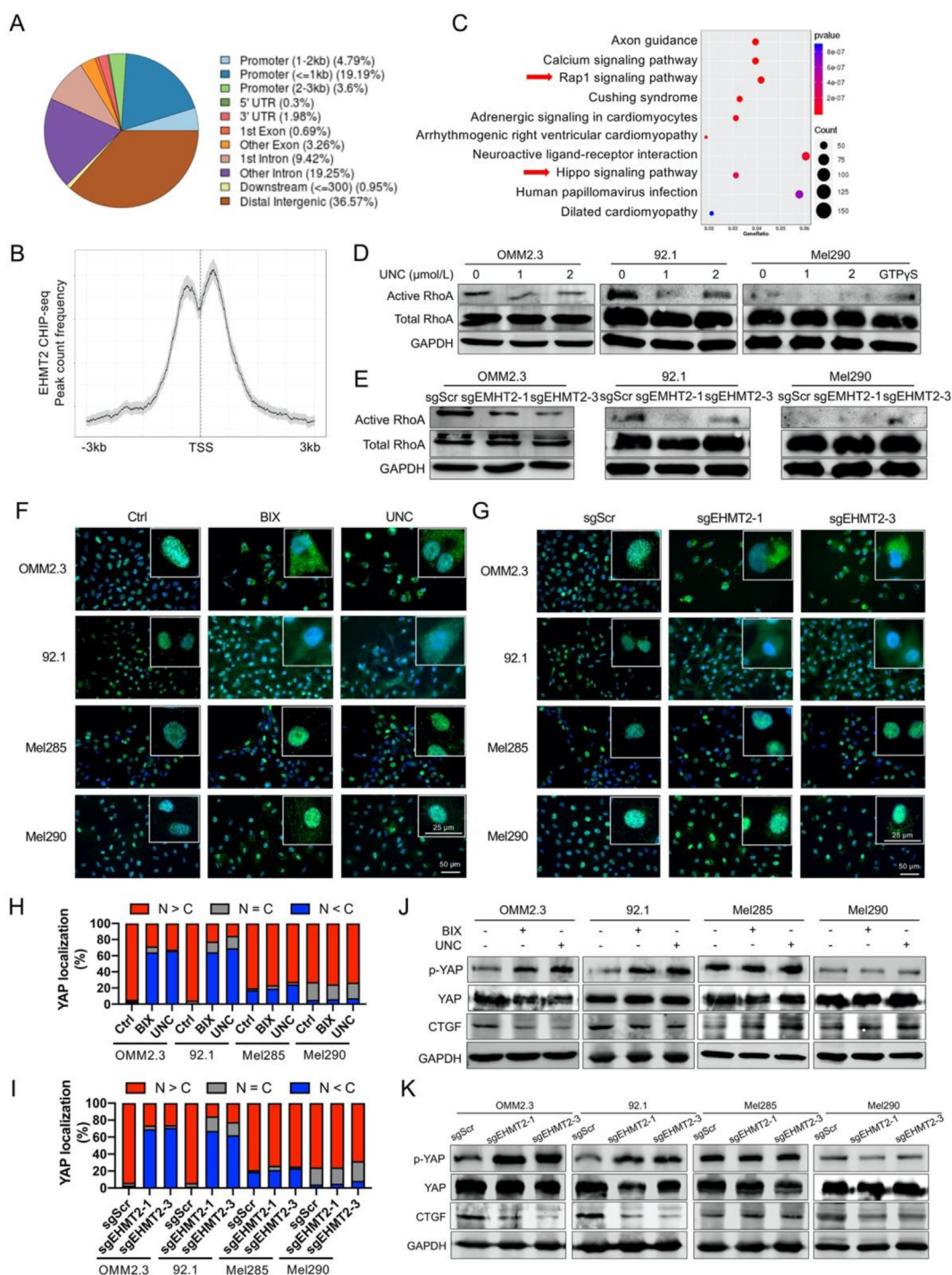


**Figure 3** Inhibiting EHMT2 blocks the activation of RhoA/YAP signaling pathway in *GNAQ11*-mutant UM. (A) Genome-wide EHMT2 occupancy is shown. (B) Histogram demonstrating the distribution of EHMT2 at TSS  $\pm$  3 kb. (C) KEGG analysis shows signaling pathways that are regulated by EHMT2. (D, E) RhoA activity is analyzed 24 h after UNC0631 (2  $\mu$ mol/L) treatment and in sgScr and sgEHMT2 UM cells. GTP $\gamma$ S is used as a positive control to activate RhoA. (F, G) Representative IF images of UM cells showing the change in YAP localization after BIX01294 (2  $\mu$ mol/L) and UNC0631 (2  $\mu$ mol/L) treatment for 24 h, as well as in sgScr and sgEHMT2 UM cells. (H, I) Relative quantification of IF assay. (J, K) WB of p-YAP, YAP and CTGF in UM cells treated with BIX01294 (2  $\mu$ mol/L) and UNC0631 (2  $\mu$ mol/L) for 24 h, as well as in sgScr and sgEHMT2 UM cells. GAPDH is used as the loading control.  $n = 3$  independent experiments for (D–G, J, K), \* $P < 0.05$ , \*\* $P < 0.01$ , \*\*\* $P < 0.001$ .

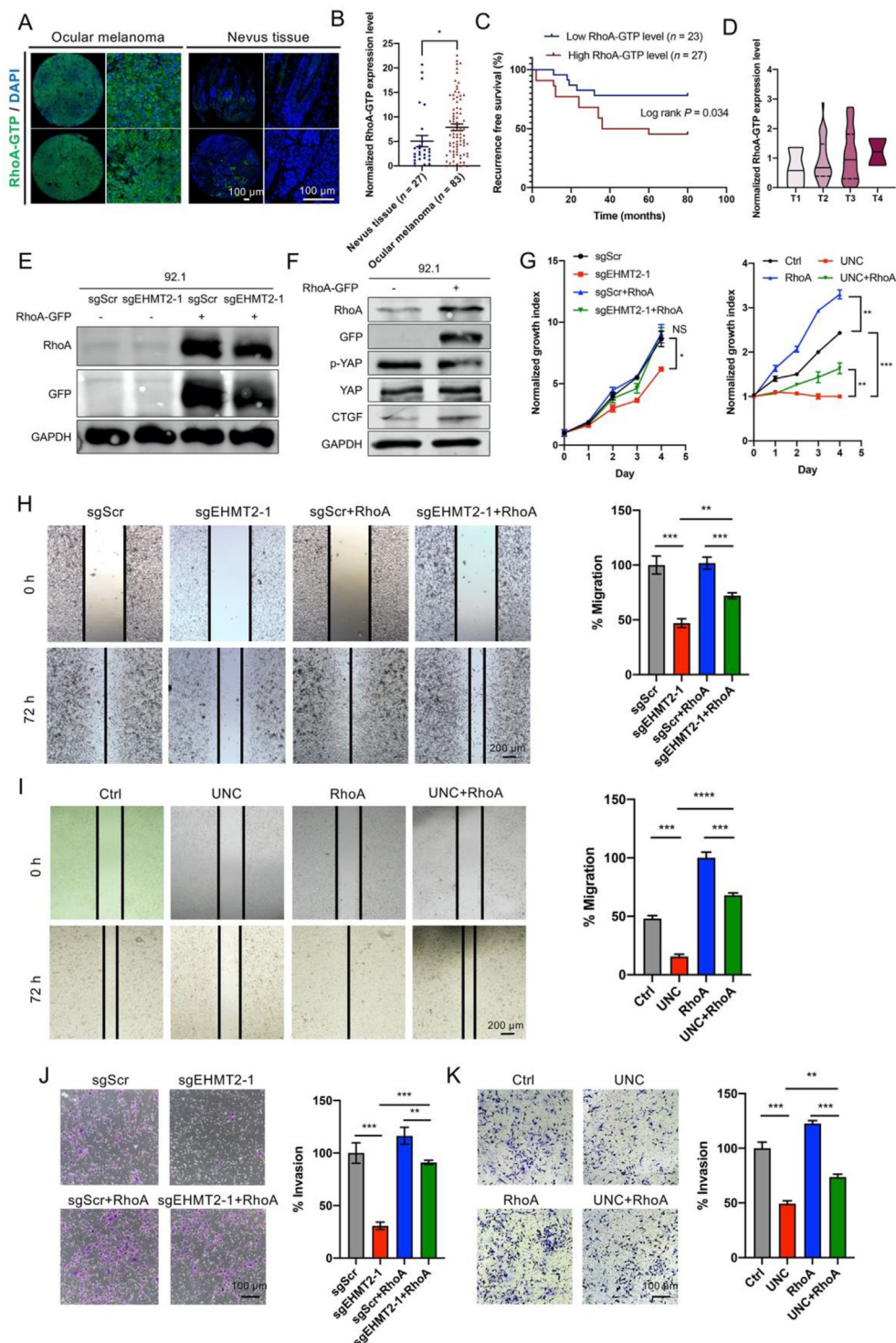


**Figure 4** RhoA is an effector of EHMT2-dependent oncogenic behaviors. (A) RhoA-GTP staining in the tissue microarray of ocular melanoma and nevus. Green represents the expression of RhoA-GTP, and blue represents DAPI. Two random cores are shown. (B) The RhoA-GTP expression level in a tissue microarray of nevus ( $n = 27$ ) and ocular melanoma ( $n = 83$ ). (C) Kaplan–Meier RFS curve of ocular melanoma patients with RhoA-GTP high-expression ( $n = 27$ ) and low-expression ( $n = 23$ ). (D) Violin diagram showing the expression level of RhoA-GTP categorized according to patients' clinical T stages. (E) sgScr and sgEHMT2-1 cells were transfected with RhoA-GFP plasmid. The expression of RhoA and GFP was determined. (F) 92.1 cells were transfected with RhoA-GFP plasmid. The expression of RhoA, GFP, p-YAP, YAP and CTGF was determined. (G) A growth curve assay is performed to measure proliferation. Wound healing assay (H, I) and Transwell assay (J, K) is done for motility. Quantification of data is shown in bar graphs. GAPDH is used as the loading control.  $n = 3$  independent experiments for (E–K),  $*P < 0.05$ ,  $**P < 0.01$ ,  $***P < 0.001$ .

activation level was related to poor RFS ( $P = 0.034$ ) and advanced T stage in a set of 83 UM patients (Fig. 4C and D).

We tested if re-introduction of constitutively active RhoA could rescue UM cell growth and migration defects previously detected in those with EHMT2i treatment and EHMT2 knock-down. The sgScr, sgEHMT2 and control 92.1 cells were transfected with empty vector (EV) or constitutively active RhoA (RhoA<sup>Q63L</sup>)-GFP plasmid (Fig. 4E and F). As expected, over-expression of active RhoA induced activation of YAP pathway and downstream target CTGF transcription (Fig. 4F). Compared with the EV group, the proliferation of sgEHMT2 and EHMT2i treated cells was significantly rescued upon introduction of exogenous

RhoA<sup>Q63L</sup>-GFP (Fig. 4G). The motility of sgEHMT2 and EHMT2i treated cells was also proved to be restored by wound healing and Transwell assays (Fig. 4–K).

### 3.5. EHMT2 directly regulates ARHGAP29 expression

As EHMT2 inhibition significantly reduced RhoA GTPase activities without affecting its expression (Fig. 3D), we wonder if other cellular factors have been involved. Because the activity of RhoA GTPase is regulated with guanine nucleotide exchange factors (GEFs) and GTPase-activating proteins (GAPs). We use ChIP-seq to profile potential GEFs and GAPs involved in the

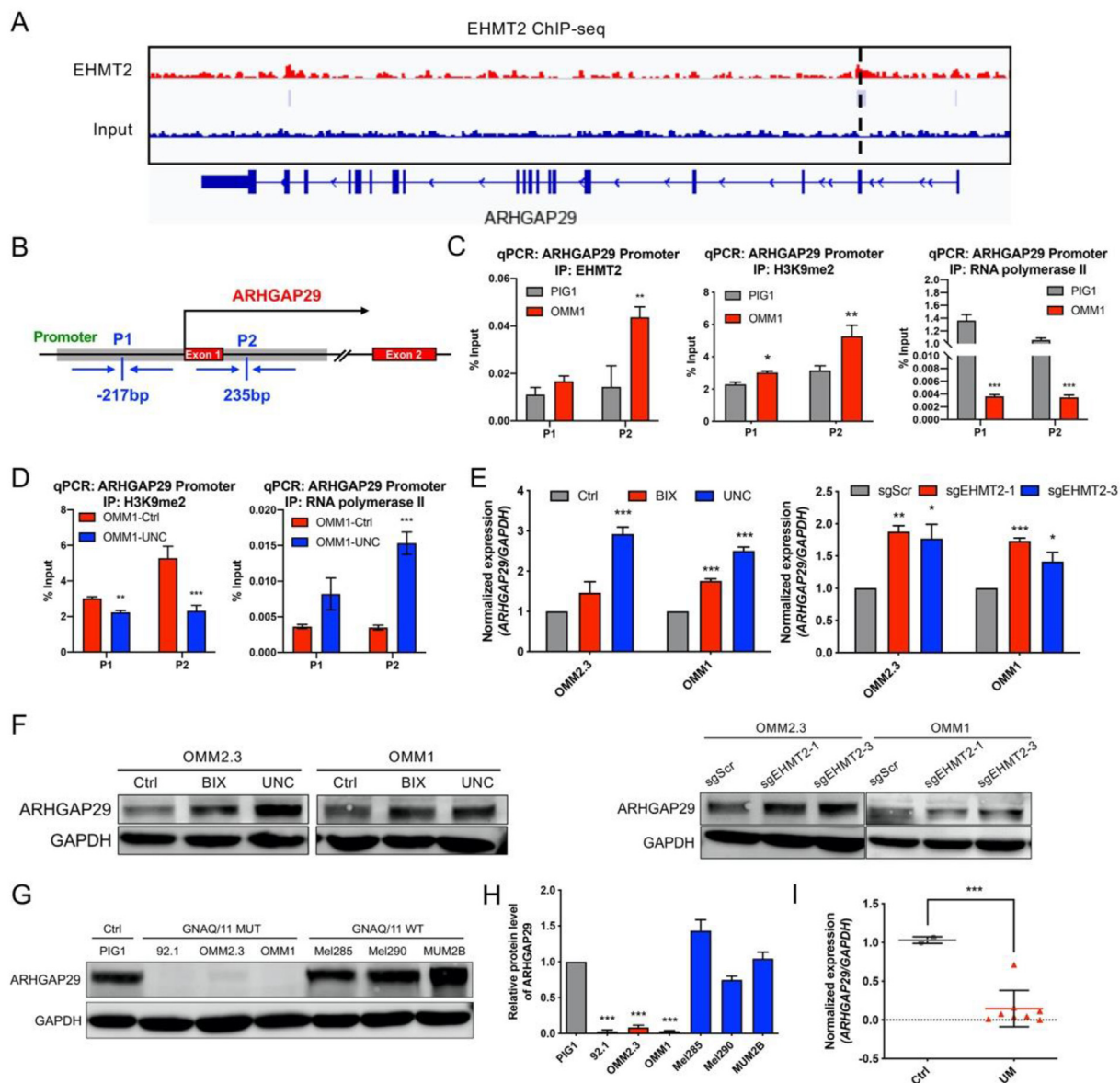


**Figure 5** *ARHGAP29* is a target gene of EHMT2. (A) Genomic snapshot showing EHMT2 enrichment at the *ARHGAP29* promoter. (B) A diagram representing the predicted promoter of *ARHGAP29* and the designed site of primers. (C) ChIP-qPCR shows EHMT2, H3K9me2 and RNA polymerase II distribution at the *ARHGAP29* promoter in PIG1 and OMM1. (D) ChIP-qPCR is done in OMM1 and UMC0631-treated (2  $\mu$ mol/L, 72 h) OMM1 for H3K9me2 and RNA polymerase II enrichment. (E, F) *ARHGAP29* mRNA and protein levels upon BIX01294/UNC0631 treatment (2  $\mu$ mol/L, 72 h), as well as in sgScr and sgEHMT2 cells, are detected by qPCR and WB in OMM2.3 and OMM1 cells. (G, H) The expression level of *ARHGAP29* is detected in one PIG1 and six UM cells and quantified with ImageJ. Quantification of data is shown in bar graphs. (I) The expression level of *ARHGAP29* mRNA is detected in eight cases of UM, as well as two control choroid tissues, via qPCR. GAPDH is used as the loading control.  $n = 3$  independent experiments for (C–G, I), \* $P < 0.05$ , \*\* $P < 0.01$ , \*\*\* $P < 0.001$ .

regulation of RhoA. The ChIP-seq data revealed that EHMT2 was enriched around the second exon region of *ARHGAP29* (Fig. 5A), which encoded a GTPase-activating protein for RhoA<sup>36</sup>. *ARHGAP29*, serving as an important modulator of actin dynamics, reduces the activity of RhoA by promoting the transformation from GTP-bound (active) RhoA to its GDP-bound (inactive) form<sup>37</sup>. In order to verify the EHMT2 genomic occupancy, two pairs of primers were designed, either before or after the first exon of *ARHGAP29* gene (Fig. 5B). The data of ChIP-qPCR showed that EHMT2 occupancy was higher in OMM1 cells compared with that in PIG1 (Fig. 5C). We then analyzed H3K9me2 and RNA polymerase II marks, representing transcriptional repression and activation respectively, on the promoter of *ARHGAP29* by ChIP-qPCR in PIG1, OMM1 and UNC0631-treated OMM1. The enrichment of H3K9me2 was stronger in OMM1 than that in PIG1 and was significantly reduced by treatment with UNC0631 (Fig. 5C and D). However, the enrichment of RNA polymerase II was much weaker in OMM1 than in PIG1 and was largely induced by treatment with UNC0631

(Fig. 5C and D). qPCR analysis revealed that *ARHGAP29* mRNA expression was elevated in UM cells with EHMT2 inhibitor treatment or stable depletion of EHMT2 (Fig. 5E). The protein level of *ARHGAP29* was also increased in UM cells with EHMT2 inhibitor treatment or EHMT2 depletion (Fig. 5F). These findings suggested an important role of EHMT2-mediated H3K9me2 for regulation of *ARHGAP29* in UM cells.

*ARHGAP29* protein expression levels in *GNAQ11*<sup>Q209</sup>-mutant cells (92.1, OMM2.3, OMM1) were much lower than that in *GNAQ11*-wild type cells (Mel285, Mel290, MUM2B) and control cell PIG1 (Fig. 5G and H). qPCR of *ARHGAP29* mRNA showed a reduced level in UM samples than in control choroid samples (Fig. 5I).

To determine the role of *ARHGAP29* in UM, we overexpressed it in 92.1 and OMM2.3, which initially did not express *ARHGAP29* (Fig. 6A). Overexpression of *ARHGAP29* inhibited RhoA and YAP signaling pathway, as showed in Fig. 6–D of downregulated active RhoA level, upregulated p-YAP level and blocked YAP nuclear translocation, respectively. By examining

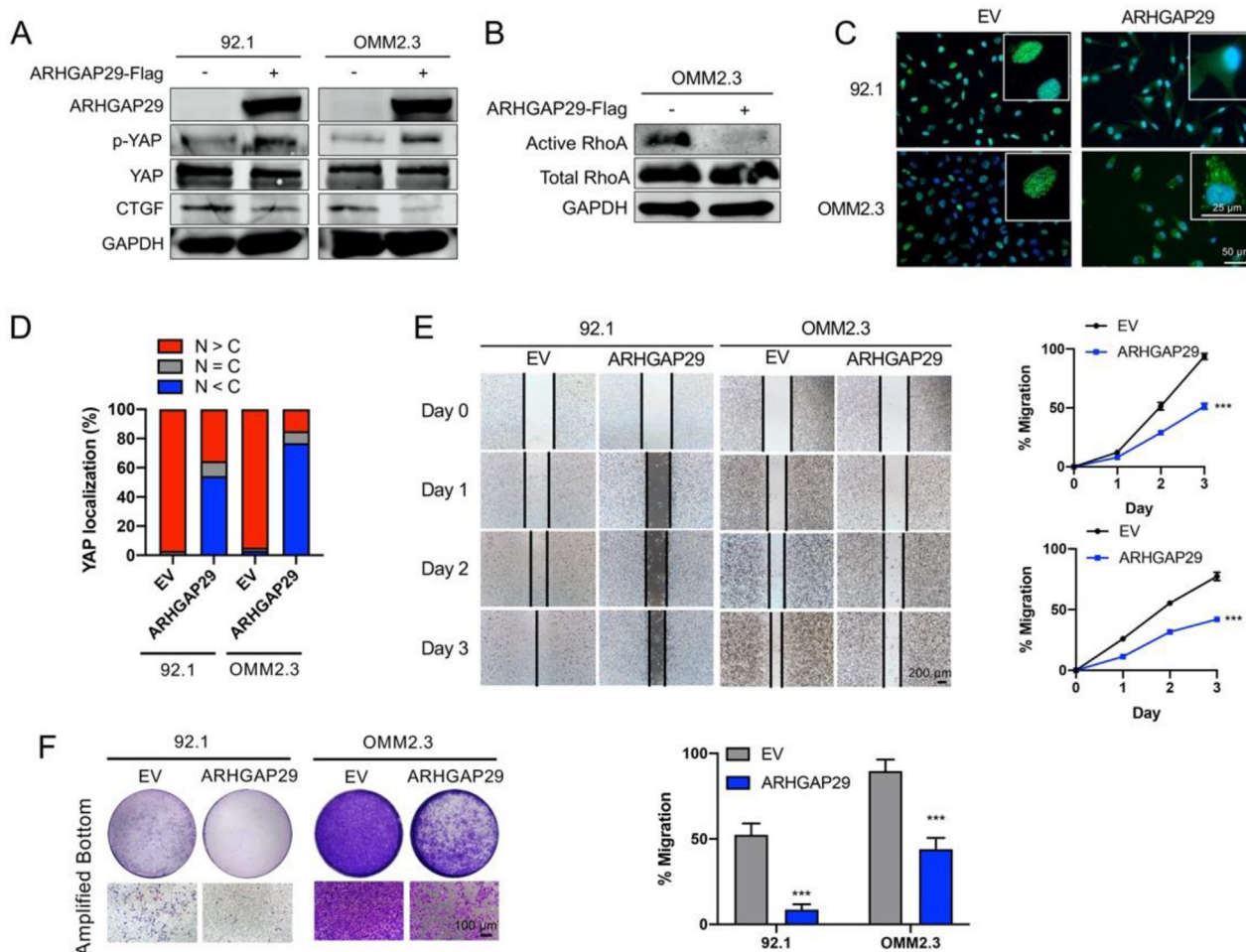


**Figure 6** *ARHGAP29* regulates RhoA pathway and cell motility. (A) 92.1 and OMM2.3 cells are transfected with *ARHGAP29*-overexpressing plasmid. Expression of *ARHGAP29*, as well as p-YAP, YAP, and CTGF, is analyzed. (B) RhoA activity is analyzed in OMM2.3 with and without *ARHGAP29* overexpression. (C) Representative IF images of 92.1 and OMM2.3 showing the change in YAP localization after *ARHGAP29* overexpression. (D) Relative quantification of IF assay. Wound healing assay (E) and Transwell assay (F) is done for motility. Quantification of data is shown in bar graphs. GAPDH is used as the loading control.  $n = 3$  independent experiments for (A–C, E, F), \* $P < 0.05$ , \*\* $P < 0.01$ , \*\*\* $P < 0.001$ .

cell migration rate 3 days post seeding *via* wound healing assay, a reduced migration was determined in UM cells with ARHGAP29 overexpression, compared with control cells (Fig. 6E). The Transwell assay had further confirmed that overexpression of ARHGAP29 reduced cell migration (Fig. 6F). Overexpression of ARHGAP29 did not affect the proliferation of UM cells. Interestingly, overexpressing ARHGAP29 also enhanced melanin synthesis which was consistent with the effect of EHMT2 depletion (Supporting Information Fig. S4A).

### 3.6. Combination of EHMT2 inhibitor and MEKi/ERKi overrides drug-resistant UM cells

To fully extend our pharmacological mapping the genetic vulnerability of *GNAQ/11*-mutant UM coupled with EHMT2 inhibition, we performed a combined drug screening with 2103 target-known drugs in OMM2.3, with or without BIX01294 co-treatment (Fig. 7A). OMM2.3 was chosen as it showed the highest MEKi-resistance with  $IC_{50}$  greater than 10  $\mu\text{mol/L}$  (Supporting Information Fig. S5A). By calculating the ratio of the number of drugs with 50% killing efficacy to the total number of drugs at the same target, 15 targets were considered to have a synergistic effect with BIX01294 (Table S1). By analyzing the normalized cellular viability, five targets were picked out (MEK, ERK, PAK, FLT3, c-Met) (Fig. 7B). In a fixed ratio/combo assay of BIX01294 and binimetinib (MEKi)/ulixertinib (ERKi), the  $IC_{50}$  of BIX01294 and kinase inhibitor was both decreased in combination (Fig. 7C, Fig. S5B and S5C). In the combination assay of variable ratio, OMM2.3 and OMM1 were applied with different concentrations of BIX01294 or binimetinib and ulixertinib, either alone or in combination. The drug synergy/antagonism was calculated *via* the HSA Additivity method. Synergistic anti-proliferative effects were determined especially at BIX01294 concentrations in range of 0–3.33  $\mu\text{mol/L}$  when combined with ulixertinib in range of 0.222–2  $\mu\text{mol/L}$  (Fig. 7D). Colony formation assay was utilized to further confirm that the anti-proliferative effect of binimetinib/ulixertinib on UM cells could be enhanced when combined with BIX01294 after prolonged treatment (Fig. 7E).

In order to evaluate the efficacy of BIX01294 combined with binimetinib/ulixertinib on UM growth *in vivo*, a zebrafish xenograft model was established. 92.1 cells carrying red fluorescence were microinjected into the yolk sac of *Tg(kdrl:egfp)<sup>la116</sup>* zebrafish at 2 days post fertilization (dpf). After six days, the growth of the UM xenograft was seen and migrated towards the eyeballs, and brain (Fig. 7F). At the safe dose of 10  $\mu\text{mol/L}$  for BIX01294, 5  $\mu\text{mol/L}$  for binimetinib and ulixertinib, CM-Dil signal in combination groups was significantly lower than that in single kinase inhibitor group ( $P < 0.001$ ) (Fig. 7G and H, Supporting Information Fig. S6). The growth and metastasis of 92.1 cells were decreased in the EHMT2 inhibitor group and combination groups.

### 3.7. *In vivo* efficacy of EHMT2 inhibitor and MEKi/ERKi

To further confirm the efficacy of EHMT2 inhibitor combined with MEKi/ERKi *in vivo*, we used two approaches. Firstly, luciferase-labeled 92.1 cells were orthotopically incubated into the eyeballs of nude mice. After 2 weeks of incubation, UNC0631 (5 mg/kg, *i.p.*, qd), binimetinib (3 mg/kg, *i.g.*, qd), and ulixertinib (50 mg/kg, *i.g.*, qd) were applied to mice either in single or in combination. The vehicle group was treated with DMSO. 21 days

after treatment, a weaker signal of UM cells was captured in the combination group, compared to single-regimen groups and vehicle group ( $P < 0.05$ ) (Fig. 8A and B). The eyeballs were filled with hyperpigmented tumor cells in the vehicle group. Residual tumors still existed in single-drug groups, while in the combination group, most eyeballs recovered to a crystal-clear situation (Fig. 8C). Weight of the whole eyes was the lowest in the combination group ( $P < 0.05$ ) (Fig. 8D). Remarkably, mice treated with single UNC0631 or in combination exhibited prolonged animal survival as compared to vehicle-treated mice and single kinase-treated mice (Fig. 8E). A significant reduction in Ki67 and increase in TUNEL staining was seen in combination groups, indicating repressed tumor cell proliferation. ARHGAP29 staining was elevated in the UNC0631-treated mice, compared to controls. The active RhoA levels were strongly downregulated (Fig. 8F).

In the second approach, a PDX model was established. Tumor volume was significantly reduced in mice administered with combined therapy (Fig. 8G). Ki67 and GTP-RhoA levels were strikingly decreased, whereas TUNEL and ARHGAP29 expression was elevated in the tumors (Fig. 8H). Taken together, inhibition of EHMT2 and MEK/ERK signaling pathway simultaneously would be an efficient treatment option for control of UM growth *in vivo*.

## 4. Discussion

Even though *GNAQ/11* has long been known as the predominated oncogenic driving force in UM, it is not an easy task like cutting off the head of the snake by directly targeting these mutant proteins. To make the situation worse, a single drug targeting PKC or MEK shows little therapeutic benefit in clinical trials, largely due to tumor cell signaling rewiring. We sought to utilize a hypothesis-generation strategy by thoroughly exploring the genetic vulnerability of *GNAQ/11*-mutant UM *via* screening a 3541 target-known compounds library. High throughput drug screening has helped us explore the biological behavior of UM cells and pharmacologically map potential druggable signaling nodes. Reverse pharmacological methods have further confirmed that elevated expression of EHMT2 suppresses the ARHGAP29 and escalates the RhoA activity in *GNAQ/11*-mutant UM.

Through the methylation of H3K9, EHMT2 can have a wide range of effects on many signal pathways, which not only depend on the tumor's own development and genetic background, but also change tumor and microenvironment cells<sup>38</sup>. Elevated expression of EHMT2 has been observed in a variety of cancers and linked to drug resistance and metastasis<sup>29</sup>. Recently, the oncogenic function of EHMT2 in cutaneous melanoma has been identified as a sort of gain-of-function *via* amplification of genomic sites or recurrent activating mutations in the SET domain<sup>39</sup>, yet its role in UM remains elusive. Through ChIP-seq analysis and ChIP-qPCR, ARHGAP29 was identified to be a downstream gene of EHMT2 in *GNAQ/11*-mutant UM. EHMT2 and H3K9me2 repressive marks at the ARHGAP29 promoter were identified. Interestingly, *GNAQ/11*-mutant UM cells all lack ARHGAP29 expression. Stable depletion of EHMT2 protein or pharmacologic inhibition both relieved the reduced ARHGAP29 expression in *GNAQ/11*-mutant cells, resulting in decreased RhoA activity, and consequently impaired proliferation and migration.

RhoA is one of the members of the Rho GTPases family participating in the regulation of cytoskeletal dynamics and intracellular signaling that contribute to the metastatic behavior of

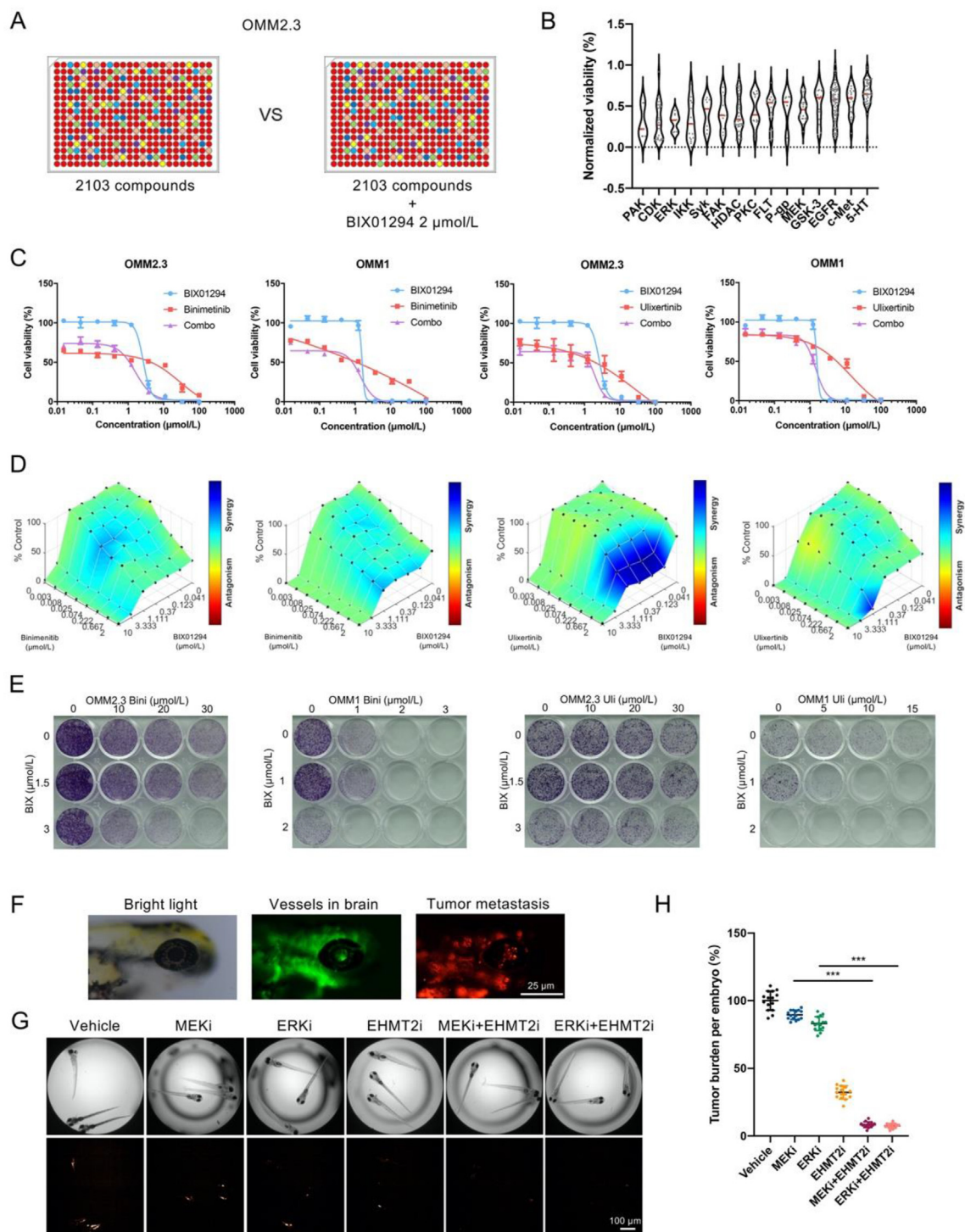


**Figure 7** Antiproliferative effect of EHMT2i on MEKi/ERKi-resistant UM cells. (A) A diagram for combined drug screening for BIX01294. (B) The violin diagram shows 15 targets having a synergistic effect with BIX01294. Each point represents cellular viability under the action of combined therapy. (C) Dose–response curves of MEKi binimetinib (MEK162), ERKi ulixertinib, EHMT2i BIX01294 and combination in UM cell lines. (D) UM cells were treated for 72 h with binimetinib, ulixertinib and BIX01294. FA values calculated at 56 diverse concentrations are demonstrated *via* Combenefit Software. (E) The colony formation of cells is observed after 14-day inoculation under single or combined treatment in different concentrations. (F) Zebrafish xenotransplantation and confocal microscope observation of UM cells. After a 6-day incubation, the metastasis of the UM xenograft can be seen in the brain. Green represents vessels in the whole body, and red represents tumor cells. (G) Representative fluorescence images of embryos microinjected with 92.1 cells and treated by BIX01294 (10  $\mu\text{mol/L}$ ), binimetinib (5  $\mu\text{mol/L}$ ) and ulixertinib (5  $\mu\text{mol/L}$ ). The image is captured at six days post treatment (dpt). (H) Quantification of tumor burden per embryo at six dpt, *via* automatic confocal analysis.  $n = 3$  independent experiments for (C–E),  $n = 15$  embryos in each group for (G), \* $P < 0.05$ , \*\* $P < 0.01$ , \*\*\* $P < 0.001$ .

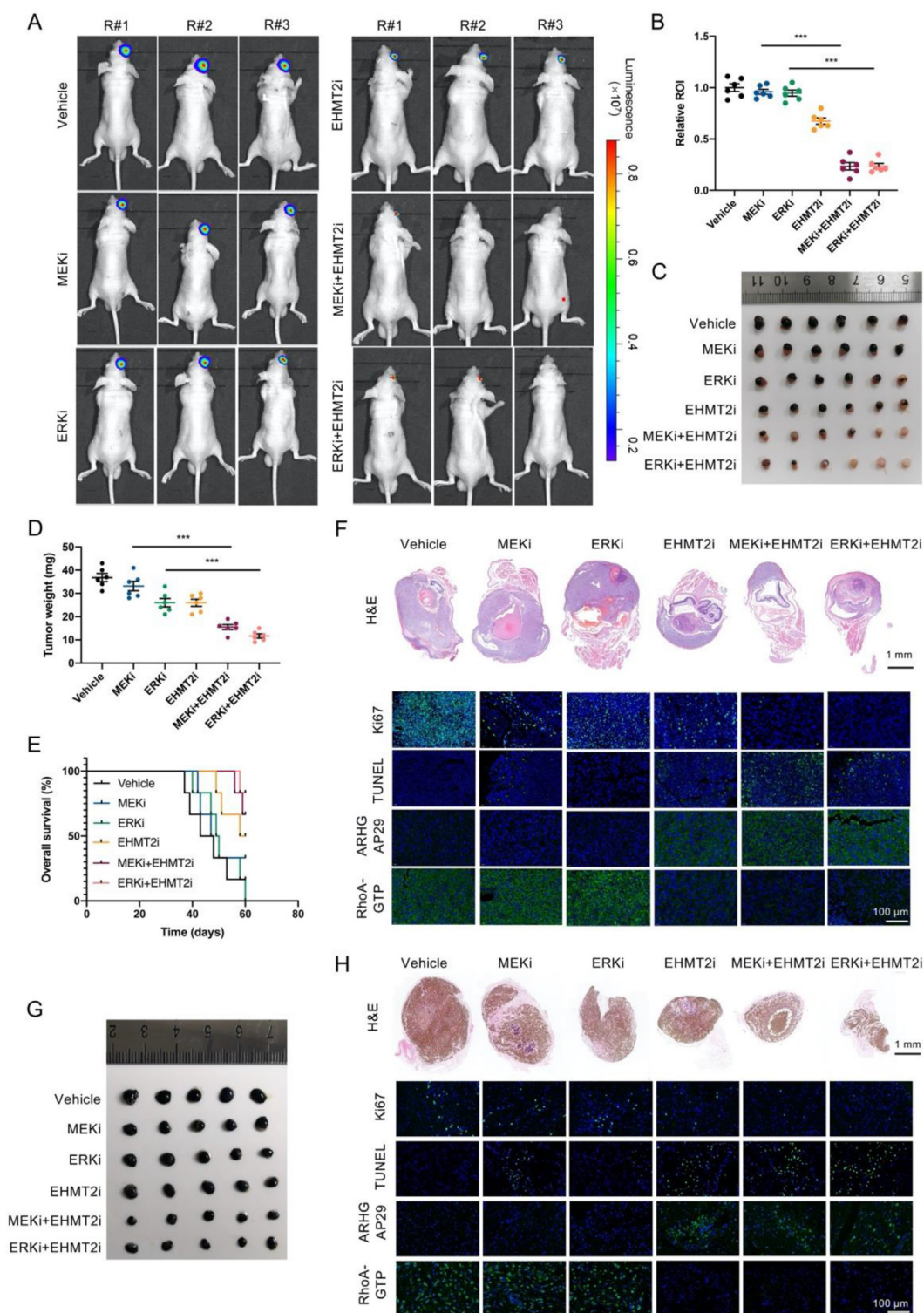


**Figure 8** EHMT2 combined with MEK/ERK inhibition impairs UM growth *in vivo*. Nude mice are injected orthotopically with 92.1 cells transfected with luciferase. After 2 weeks, mice are treated with either vehicle DMSO, binimetinib (3 mg/kg, qd), ulixertinib (50 mg/kg, qd), UNC0631 (5 mg/kg, qd), or in combination. The tumor bioluminescent signal (A) and quantification (B) of 92.1 in orthotopic xenografts are recorded 21 days after treatment. (C) Tumors are collected after 21-day treatment. (D) The weight of the eyes is measured 21 days after treatment. (E) Kaplan–Meier survival plot for xenograft mice in six groups. Representative images of H&E staining (F), as well as Ki67, TUNEL, ARHGAP29 and RhoA-GTP expression determined by IF. (G) PDX models are established by planting UM tissues subcutaneously in nude mice. Mice are treated with either vehicle DMSO, binimetinib (3 mg/kg, qd), ulixertinib (50 mg/kg, qd), UNC0631 (5 mg/kg, qd), or in combination. Tumors are harvested after 21-day treatment. Representative images of H&E staining (H), as well as Ki67, TUNEL, ARHGAP29 and RhoA-GTP levels assessed by IF in the tumor tissues.  $n = 6$  mice in each group for (A, G),  $*P < 0.05$ ,  $**P < 0.01$ ,  $***P < 0.001$ .

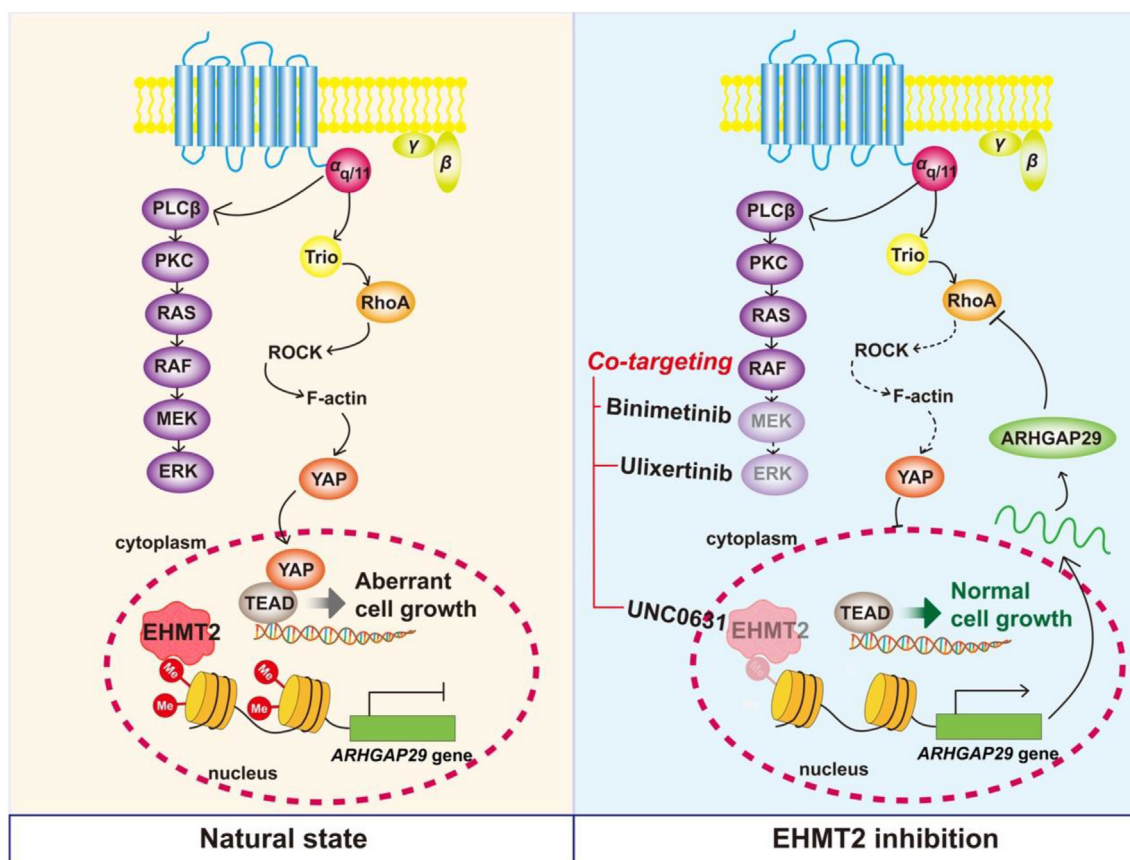


**Figure 9** A schematic picture for this study. A schematic picture of the mechanism of how EHMT2i targets *GNAQ11*-mutant UM.  $G\alpha_{q11}$ /Trio/RhoA/YAP pathway is continuously activated in UM. EHMT2, together with H3K9me2, could bind with the promoter region of the *ARHGAP29* gene and inhibit its transcription, resulting in the continuous activation of RhoA. By using an EHMT2 inhibitor or stably knocking down EHMT2, the expression of ARHGAP29 can be rescued. Then, RhoA turns from the activated state (RhoA-GTP) to inactivated state (RhoA-GDP), thus blocking the downstream YAP pathway, to inhibit the progression of UM. EHMT2 combined with MEKi/ERKi is a novel therapeutic approach for UM.

cancer cells<sup>40</sup>. Inhibition of Rho-associated protein kinase in UM, one of the downstream effectors of activated RhoA, represses the amoeboid blebbing capacity<sup>41</sup>. It has been reported that ARHGAP29 inactivates RhoA<sup>42,43</sup>. A previous study showed that the single nucleotide polymorphisms altering the binding of the *ARHGAP29* promoter with transcription factors could affect the activity of *ARHGAP29* enhancers<sup>44</sup>. Meanwhile, *ARHGAP29* expression was derepressed by EHMT2 inhibitor UNC0631, which correlated with reduced RhoA activity. We revealed RhoA signaling was activated in ocular melanoma in comparison with nevus, and its high activation level was associated with poorer RFS and more advanced T stage of patients. Re-expression of constitutively active RhoA could restore the proliferative and motility activity of sgEHMT2 cells. Taken together, the data suggest that ARHGAP29 loses its function to inactivate RhoA and consequently promotes UM cell migration.

Many preclinic and clinical studies indicate that the treatment of UM may require combined therapy. Here we fully explore the potential synergistic effect in killing UM cells between EHMT2 inhibitors and various kinds of kinase inhibitors. Among them, the synergistic effect between BIX01294 and inhibitors targeting MEK, ERK, PAK, FLT3 and c-Met was the most prominent. A similar combination strategy of epigenetic compounds and kinase inhibitors has been recommended before. For example, inhibiting

HDAC3 enhances the efficacy of MAPK pathway inhibitors in melanoma<sup>45</sup>. In UM, adaptive YAP activation and AKT signaling are key pathways involved in the escape of tumor cells from MEK inhibition, which could be suppressed by adding HDAC inhibitors<sup>46</sup>. Based on our findings, as well as the recent bioinformatics analysis implicating important methyltransferases and acetyltransferases in cancers, we propose EHMT2 combined with MEKi/ERKi as a promising therapeutic approach for UM.

## 5. Conclusions

In summary, we find that methyltransferase EHMT2 is upregulated in UM. EHMT2 inhibitors suppress *GNAQ11*-mutant UM cell growth and invasiveness through regulating the expression of GTPase-activating protein ARHGAP29 and the activity of RhoA/YAP signaling pathway (Fig. 9). Our findings suggest an effective strategy for UM intervention by inhibiting EHMT2 and MEKi/ERK signaling simultaneously.

## Acknowledgments

This research was supported by the Science and Technology Commission of Shanghai (20DZ2270800, China), the National

Natural Science Foundation of China (grants 82073889), the Innovative Research Team of High-level Local Universities in Shanghai (SHSMU-ZDCX20210900, China), China Postdoctoral Science Foundation (2022M722120, China) and Shanghai Sailing Program (22YF1422800, China). The funders had no role in the study design, data collection and analysis, decision to publish, or the preparation of the manuscript.

### Author contributions

Jianming Zhang, Yongyun Li, Tianyu Zhu, and Jie Yang designed and performed the experiments; Jie Yang, Tianyu Zhu, and Shengfang Ge were responsible for the animal model; Yongyun Li and Qianqian Zhang conducted HTS; Yongyun Li, Shiqiong Xu, and Renbing Jia analyzed the data; Yongyun Li, Jianming Zhang and Xianqun Fan drafted the paper. All authors read and approved the final paper.

### Conflicts of interest

The authors declare no competing interests.

### Appendix A. Supporting information

Supporting data to this article can be found online at <https://doi.org/10.1016/j.apsb.2023.12.002>.

### References

- Jager MJ, Shields CL, Cebulla CM, Abdel-Rahman MH, Grossniklaus HE, Stern MH, et al. Uveal melanoma. *Nat Rev Dis Prim* 2020;**6**:24.
- Li Y, Shi J, Yang J, Ge S, Zhang J, Jia R, et al. Uveal melanoma: progress in molecular biology and therapeutics. *Ther Adv Med Oncol* 2020;**12**:1758835920965852.
- Shields JA, Shields CL. Management of posterior uveal melanoma: past, present, and future: the 2014 Charles L. Schepens lecture. *Ophthalmology* 2015;**122**:414–28.
- Khoja L, Atenafu EG, Suci S, Leyvraz S, Sato T, Marshall E, et al. Meta-analysis in metastatic uveal melanoma to determine progression free and overall survival benchmarks: an international rare cancers initiative (IRCI) ocular melanoma study. *Ann Oncol* 2019;**30**:1370–80.
- Smit KN, Jager MJ, de Klein A, Kili E. Uveal melanoma: towards a molecular understanding. *Prog Retin Eye Res* 2020;**75**:100800.
- Van Raamsdonk CD, Griewank KG, Crosby MB, Garrido MC, Vemula S, Wiesner T, et al. Mutations in GNA11 in uveal melanoma. *N Engl J Med* 2010;**363**:2191–9.
- Offermanns S, Simon MI. Genetic analysis of mammalian G-protein signalling. *Oncogene* 1998;**17**:1375–81.
- Schrage R, Schmitz AL, Gaffal E, Annala S, Kehraus S, Wenzel D, et al. The experimental power of FR900359 to study Gq-regulated biological processes. *Nat Commun* 2015;**6**:10156.
- Onken MD, Makepeace CM, Kaltenbronn KM, Kanai SM, Todd TD, Wang S, et al. Targeting nucleotide exchange to inhibit constitutively active G protein alpha subunits in cancer cells. *Sci Signal* 2018;**11**:ea06852.
- Ge Y, Deng JJ, Zhu J, Liu L, Ouyang S, Song Z, et al. Discovery of small molecule Galphaq/11 protein inhibitors against uveal melanoma. *Acta Pharm Sin B* 2022;**12**:3326–40.
- Ge Y, Shi S, Deng JJ, Chen XP, Song Z, Liu L, et al. Design, synthesis, and evaluation of small molecule Galphaq/11 protein inhibitors for the treatment of uveal melanoma. *J Med Chem* 2021;**64**:3131–52.
- Steeb T, Wessely A, Ruzicka T, Heppt MV, Berking C. How to MEK the best of uveal melanoma: a systematic review on the efficacy and safety of MEK inhibitors in metastatic or unresectable uveal melanoma. *Eur J Cancer* 2018;**103**:41–51.
- Feng X, Degese MS, Iglesias-Bartolome R, Vaque JP, Molinolo AA, Rodrigues M, et al. Hippo-independent activation of YAP by the GNAQ uveal melanoma oncogene through a trio-regulated rho GTPase signaling circuitry. *Cancer Cell* 2014;**25**:831–45.
- Li Y, Yang J, Zhang Q, Xu S, Sun W, Ge S, et al. Copper ionophore elesclomol selectively targets GNAQ/11-mutant uveal melanoma. *Oncogene* 2022;**41**:3539–53.
- Yu FX, Luo J, Mo JS, Liu G, Kim YC, Meng Z, et al. Mutant Gq/11 promote uveal melanoma tumorigenesis by activating YAP. *Cancer Cell* 2014;**25**:822–30.
- Herwig-Carl MC, Sharma A, Holler T, Holz FG, Schlitter AM, Loeffler KU. Spatial intratumor heterogeneity in uveal melanoma: tumor cell subtypes with a presumed invasive potential exhibit a particular epigenetic staining reaction. *Exp Eye Res* 2019;**182**:175–81.
- Souri Z, Jochemsen AG, Wierenga APA, Kroes WGM, Verdijk RM, van der Velden PA, et al. Expression of HDACs 1, 3 and 8 is upregulated in the presence of infiltrating lymphocytes in uveal melanoma. *Cancers* 2021;**13**:4146.
- Holling TM, Bergevoet MW, Wilson L, Van Eggermond MC, Schooten E, Steenbergen RD, et al. A role for EZH2 in silencing of IFN-gamma inducible MHC2TA transcription in uveal melanoma. *J Immunol* 2007;**179**:5317–25.
- Jin B, Zhang P, Zou H, Ye H, Wang Y, Zhang J, et al. Verification of EZH2 as a druggable target in metastatic uveal melanoma. *Mol Cancer* 2020;**19**:52.
- De Waard-Siebinga I, Blom DJ, Griffioen M, Schrier PI, Hoogendoorn E, Beverstock G, et al. Establishment and characterization of an uveal-melanoma cell line. *Int J Cancer* 1995;**62**:155–61.
- Chen PW, Murray TG, Uno T, Salgaller ML, Reddy R, Ksander BR. Expression of MAGE genes in ocular melanoma during progression from primary to metastatic disease. *Clin Exp Metastasis* 1997;**15**:509–18.
- Luyten GP, Naus NC, Mooy CM, Hagemeyer A, Kan-Mitchell J, Van Druenen E, et al. Establishment and characterization of primary and metastatic uveal melanoma cell lines. *Int J Cancer* 1996;**66**:380–7.
- Ksander BR, Rubsamen PE, Olsen KR, Cousins SW, Streilein JW. Studies of tumor-infiltrating lymphocytes from a human choroidal melanoma. *Invest Ophthalmol Vis Sci* 1991;**32**:3198–208.
- Amirouchene-Angelozzi N, Nemati F, Gentien D, Nicolas A, Dumont A, Carita G, et al. Establishment of novel cell lines recapitulating the genetic landscape of uveal melanoma and preclinical validation of mTOR as a therapeutic target. *Mol Oncol* 2014;**8**:1508–20.
- Seftor EA, Meltzer PS, Kirschmann DA, Pe'er J, Maniotis AJ, Trent JM, et al. Molecular determinants of human uveal melanoma invasion and metastasis. *Clin Exp Metastasis* 2002;**19**:233–46.
- Le Poole IC, van den Berg FM, van den Wijngaard RM, Galloway DA, van Amstel PJ, Buffing AA, et al. Generation of a human melanocyte cell line by introduction of HPV16 E6 and E7 genes. *In Vitro Cell Dev Biol Anim* 1997;**33**:42–9.
- Jia R, Chai P, Wang S, Sun B, Xu Y, Yang Y, et al. m(6)A modification suppresses ocular melanoma through modulating HINT2 mRNA translation. *Mol Cancer* 2019;**18**:161.
- Maeda R, Tachibana M. HP1 maintains protein stability of H3K9 methyltransferases and demethylases. *EMBO Rep* 2022;**23**:e53581.
- Haebe JR, Bergin CJ, Sandouka T, Benoit YD. Emerging role of G9a in cancer stemness and promises as a therapeutic target. *Oncogenesis* 2021;**10**:76.
- Wei L, Chiu DK, Tsang FH, Law CT, Cheng CL, Au SL, et al. Histone methyltransferase G9a promotes liver cancer development by epigenetic silencing of tumor suppressor gene RARRES3. *J Hepatol* 2017;**67**:758–69.
- Bhat AV, Palanichamy Kala M, Rao VK, Pignata L, Lim HJ, Suriyamurthy S, et al. Epigenetic regulation of the PTEN-AKT-RAC1

- axis by G9a is critical for tumor growth in alveolar rhabdomyosarcoma. *Cancer Res* 2019;**79**:2232–43.
32. Ma W, Han C, Zhang J, Song K, Chen W, Kwon H, et al. The Histone methyltransferase G9a promotes cholangiocarcinogenesis through regulation of the Hippo pathway kinase LATS2 and YAP signaling pathway. *Hepatology* 2020;**72**:1283–97.
  33. Phelps GB, Hagen HR, Amsterdam A, Lees JA. MITF deficiency accelerates GNAQ-driven uveal melanoma. *Proc Natl Acad Sci U S A* 2022;**119**:e2107006119.
  34. Post A, Pannekoek WJ, Ross SH, Verlaan I, Brouwer PM, Bos JL. Rasip1 mediates Rap1 regulation of Rho in endothelial barrier function through ArhGAP29. *Proc Natl Acad Sci U S A* 2013;**110**:11427–32.
  35. Zhang J, Liu S, Ye Q, Pan J. Transcriptional inhibition by CDK7/9 inhibitor SNS-032 abrogates oncogene addiction and reduces liver metastasis in uveal melanoma. *Mol Cancer* 2019;**18**:140.
  36. Tagashira T, Fukuda T, Miyata M, Nakamura K, Fujita H, Takai Y, et al. Afadin facilitates vascular endothelial growth factor-induced network formation and migration of vascular endothelial cells by inactivating Rho-associated kinase through ArhGAP29. *Arterioscler Thromb Vasc Biol* 2018;**38**:1159–69.
  37. Sun Y, Leng P, Guo P, Gao H, Liu Y, Li C, et al. G protein coupled estrogen receptor attenuates mechanical stress-mediated apoptosis of chondrocyte in osteoarthritis via suppression of Piezo1. *Mol Med* 2021;**27**:96.
  38. Flesher JL, Fisher DE. G9a: an emerging epigenetic target for melanoma therapy. *Epigenomes* 2021;**5**:23.
  39. Kato S, Weng QY, Insko ML, Chen KY, Muralidhar S, Pozniak J, et al. Gain-of-function genetic alterations of G9a drive oncogenesis. *Cancer Discov* 2020;**10**:980–97.
  40. Jansen S, Gosens R, Wieland T, Schmidt M. Paving the rho in cancer metastasis: rho GTPases and beyond. *Pharmacol Ther* 2018;**183**:1–21.
  41. Onken MD, Blumer KJ, Cooper JA. Uveal melanoma cells use amoeboid and mesenchymal mechanisms of cell motility crossing the endothelium. *Mol Biol Cell* 2021;**32**:413–21.
  42. Saras J, Franzen P, Aspenstrom P, Hellman U, Gonez LJ, Heldin CH. A novel GTPase-activating protein for Rho interacts with a PDZ domain of the protein-tyrosine phosphatase PTPL1. *J Biol Chem* 1997;**272**:24333–8.
  43. Barry DM, Koo Y, Norden PR, Wylie LA, Xu K, Wichaidit C, et al. Rasip1-mediated Rho GTPase signaling regulates blood vessel tubulogenesis via nonmuscle Myosin II. *Circ Res* 2016;**119**:810–26.
  44. Liu H, Leslie EJ, Carlson JC, Beaty TH, Marazita ML, Lidral AC, et al. Identification of common non-coding variants at 1p22 that are functional for non-syndromic orofacial clefting. *Nat Commun* 2017;**8**:14759.
  45. Lombard DB, Cierpicki T, Grembecka J. Combined MAPK pathway and HDAC inhibition breaks melanoma. *Cancer Discov* 2019;**9**:469–71.
  46. Faiao-Flores F, Emmons MF, Durante MA, Kinose F, Saha B, Fang B, et al. HDAC inhibition enhances the *in vivo* efficacy of MEK inhibitor therapy in uveal melanoma. *Clin Cancer Res* 2019;**25**:5686–701.